J. Fluid Mech. (1987), *vol.* 182, *pp.* 149–168
Printed in Great Britain

Inviscid flow about a cylinder rising to a free surface

By JOHN G. TELSTE
David W. Taylor Naval Ship Research and Development Center,
Bethesda, MD 20084-5000, USA

(Received 15 July 1986 and in revised form 16 December 1986)

The problem of calculating nonlinear two-dimensional free-surface potential flow about a circular cylinder rising to a free surface is solved numerically. The deeply-submerged circular cylinder is accelerated smoothly from rest to a uniform vertical velocity. A boundary/integral-equation method is used to obtain free-surface elevations and streamlines about the rising cylinder for several final speeds. Results, including pressure forces, are compared with a cylinder rising to a rigid wall and a cylinder moving in an infinite fluid.

1. Introduction

Substantial progress has been made in the simulation of fully nonlinear two-dimensional potential flows about objects moving near a free surface. In particular, Haussling & Coleman (1979) have studied water waves generated by a horizontally accelerated circular cylinder, and Baker, Meiron & Orszag (1981) have simulated the flow about a translating ellipse under a free surface. Lin, Newman & Yue (1984) have numerically modelled flows about bodies moving in a free surface and have paid particular attention to the intersection of the free surface with the bodies. Greenhow & Lin (1985) have used the method of Vinje & Brevig (1981) and treated the intersection of the free surface and the body in a manner suggested by Lin *et al.* (1984). These papers dealing with the intersection point are heading toward a local jet-flow model of the flow near the free-surface/body intersection which is to be matched with the potential flow solution elsewhere in the fluid. This model of singular flow near the intersection point is not yet complete.

This paper describes the results of a numerical study of the potential flow about a circular cylinder as it rises and nears a free surface. The cylinder is accelerated to a uniform vertical velocity and moves to within a distance from the free surface which is a small fraction of its diameter. This problem contains a much stronger body/free-surface interaction than those treated by Haussling & Coleman (1979) and Baker *et al.* (1981). Yet it avoids the still to be overcome free-surface/body intersection problems. This work covers the initial part of the cylinder-exit problem studied experimentally by Greenhow & Lin (1983). The flow is studied for various speeds of approach to the surface. Streamlines, the pressure distribution on the cylinder, and the total force on the cylinder are compared for the different approach speeds. The results are compared with the potential flow about a cylinder rising to a rigid wall and about a cylinder moving in an infinite fluid.

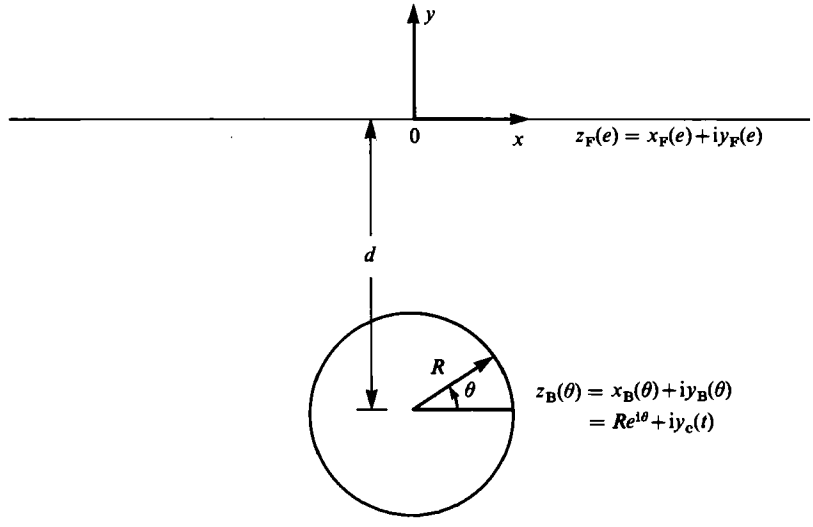

FIGURE 1. Definition Sketch.

2. Mathematical formulation

The problem considered is the calculation of the two-dimensional flow about a circular cylinder as it rises towards a free surface. The cylinder is accelerated smoothly from rest to a final vertical velocity. The fluid is assumed to be incompressible, inviscid, initially at rest, and to fill a time-dependent region which is infinite in depth and lateral extent. In addition, the fluid motion is assumed to be irrotational and surface tension is neglected. A Cartesian coordinate system is fixed so that the y-axis point vertically upward, the x-axis lies in the undisturbed free-surface, and the origin lies directly above the centre of the cylinder (figure 1).

All variables have been non-dimensionalized. Lengths have been scaled by the radius R of the cylinder; velocities, by the final speed U of the cylinder; and time, by R/U. The location of the free-surface boundary $\partial\Omega_F$ is unknown and must be computed as part of the solution. The motion of the cylinder, whose boundary is $\partial\Omega_B$, is prescribed. The assumptions guarantee the existence of a velocity potential ϕ in the time-dependent fluid region $\Omega(t)$. This potential satisfies an initial/boundary-value problem given by the following equations, which have been used by Longuet-Higgins & Cokelet (1976) and others:

$$\phi_{xx} + \phi_{yy} = 0 \quad \text{in } \Omega(t), \tag{1}$$

$$\frac{Dx}{Dt} = \phi_x \quad \text{on } \partial\Omega_F, \tag{2}$$

$$\frac{Dy}{Dt} = \phi_y \quad \text{on } \partial\Omega_F, \tag{3}$$

$$\frac{D\phi}{Dt} = \tfrac{1}{2}(\phi_x^2 + \phi_y^2) - \frac{y}{Fr^2} \quad \text{on } \partial\Omega_F, \tag{4}$$

$$\nabla\phi \cdot \boldsymbol{n} = \dot{y}_c(t)\, n_y \quad \text{on } \partial\Omega_B, \tag{5}$$

$$\phi_x = 0 \quad \text{for } x = \pm\infty, (x, y) \quad \text{in } \Omega(t), \tag{6}$$

$$\phi_y = 0 \quad \text{for } -\infty < x < \infty, \quad y = -\infty, \tag{7}$$

$$\phi(t=0) = 0 \quad \text{for } (x, y) \quad \text{in } \Omega(t=0), \tag{8}$$

$$y(t=0) = 0 \quad \text{on } \partial\Omega_{\mathrm{F}}(t=0). \tag{9}$$

The subscripts x and y denote partial differentiation with respect to these variables, and the derivative $\mathrm{D}/\mathrm{D}t$ denotes a material derivative. The Froude number is $Fr = U/(gR)^{\frac{1}{2}}$. The vector $\boldsymbol{n} = (n_x, n_y)$ is the unit normal vector at the cylinder directed into the fluid. The centre of the cylinder is at $(x = 0, y = y_{\mathrm{c}}(t))$ in which

$$y_{\mathrm{c}}(0) = -d, \tag{10}$$

$$\dot{y}_{\mathrm{c}}(t) = \sin(\tfrac{1}{2}\pi t) \quad \text{for } 0 \leqslant t \leqslant 1, \tag{11}$$

$$\dot{y}_{\mathrm{c}}(t) = 1 \quad \text{for } t \geqslant 1, \tag{12}$$

where d is the initial depth of the centre of the cylinder. The pressure on the cylinder is obtained from Bernoulli's equation

$$p = -\phi_t - \tfrac{1}{2}(\phi_x^2 + \phi_y^2) - \frac{y}{Fr^2}, \tag{13}$$

in which the subscript t denotes partial differentiation with respect to t and p is the pressure normalized by ρU^2 where ρ is the fluid density.

For comparison with the free-surface flow, the two-dimensional potential flow is computed for the circular cylinder approaching a rigid wall. For this case the initial/boundary-value problem for the velocity potential is still specified by (1), (5)–(8), and (10)–(12), but the free-surface conditions (2)–(4) are replaced by the wall condition

$$\phi_y = 0 \quad \text{at } y = 0. \tag{14}$$

The formula for the pressure on the cylinder remains the same.

The dynamic pressure p_{d} is obtained by excluding the hydrostatic pressure. Thus, it is obtained from (13) by excluding the last term:

$$p_{\mathrm{d}} = -\phi_t - \tfrac{1}{2}(\phi_x^2 + \phi_y^2). \tag{15}$$

The total vertical force F, normalized by $\rho U^2 R$, is given in terms of the dynamic pressure by the formula

$$F = -\int_0^{2\pi} p_{\mathrm{d}}(\theta) \sin\theta \, \mathrm{d}\theta + \frac{\pi}{Fr^2}, \tag{16}$$

in which the first term represents the dynamic force acting on the cylinder and the second term is the buoyancy force.

3. Method of solution

The initial/boundary-value problem is solved by the generalized vortex method of Baker, Meiron & Orszag (1981, 1982). In this method, the velocity potential is represented in terms of a distribution of vortices on the free surface and a distribution of sources on the cylinder. Specifically, the free surface and the vortex distribution on it are parameterized in terms of the time t and a parameter e as $z_{\mathrm{F}}(e, t) = x_{\mathrm{F}}(e, t) + \mathrm{i}y_{\mathrm{F}}(e, t)$ and $\gamma(e, t)$; the cylinder contour and the source distribution

on it are parameterized in terms of t and an angle θ as $z_B(\theta, t) = x_B(\theta, t) + iy_B(\theta, t)$ and $\sigma(\theta, t)$ in which

$$x_B(\theta, t) = \cos\theta, \tag{17}$$

$$y_B(\theta, t) = y_c(t) + \sin\theta. \tag{18}$$

Here $-\infty < e < \infty$, $0 \leqslant \theta \leqslant 2\pi$, and $t \geqslant 0$. Thus, the complex velocity potential $w(z) = \phi + i\psi$ at $z = x + iy$ in the fluid region $\Omega(t)$ is written as

$$w(z) = \frac{1}{2\pi i}\int_{-\infty}^{\infty} \gamma(e') \log(z - z_F(e'))\, de' + \frac{1}{2\pi}\int_0^{2\pi} \sigma(\theta') \log(z - z_B(\theta'))\, d\theta', \tag{19}$$

where ϕ is the velocity potential and ψ is the stream function. A principal-value velocity $q(e) = u(e) + iv(e)$, in which $u(e)$ is the x-component and $v(e)$ is the y-component of the velocity, is defined at any point e on the free surface by the equation

$$q^*(e) = \frac{1}{2\pi i}\int_{-\infty}^{\infty} \frac{\gamma(e')}{z_F(e) - z_F(e')}\, de' + \frac{1}{2\pi}\int_0^{2\pi} \frac{\sigma(\theta')}{z_F(e) - z_B(\theta')}\, d\theta', \tag{20}$$

where the asterisk denotes complex conjugation. The physical velocity of a point $z_F(e, t)$ on the free surface is defined by

$$\frac{\partial z_{F^*}}{\partial t}(e, t) \equiv \tilde{q}^*(e) = q^*(e) + \frac{\gamma(e)}{2(z_F(e, t))_e} \tag{21}$$

and coincides with the fluid velocity at the point. The subscript e denotes partial differentiation with respect to e. Application of the dynamic free-surface boundary condition (4) and the body boundary condition (5) to (19) leads to the two evolution equations for γ and σ:

$$\frac{\partial \gamma}{\partial t}(e) = \frac{1}{4}\frac{\partial}{\partial e}\left(\frac{\gamma^2}{(z_F)_e (z_F)_e^*}\right) - 2\left[Re\left\{\frac{\partial q^*}{\partial t}(z_F)_e - \frac{\gamma}{2}\frac{q_e}{(z_F)_e}\right\} + \frac{(y_F)_e}{Fr^2}\right], \tag{22}$$

$$\frac{\partial \sigma}{\partial t}(\theta) = 2\ddot{y}_c \sin(\theta) + Re\left\{\frac{z_B'(\theta)}{\pi}\left[\int_{-\infty}^{\infty} \frac{\partial\gamma/\partial t(e')}{z_B(\theta) - z_F(e')}\, de' + i\int_0^{2\pi} \frac{\partial\sigma/\partial t(\theta')}{z_B(\theta) - z_B(\theta')}\, d\theta' - \int_{-\infty}^{\infty} \gamma(e') \frac{\dot{z}_B(\theta) - \tilde{q}(e')}{[z_B(\theta) - z_F(e')]^2}\, de'\right]\right\}. \tag{23}$$

The functions q_e and $\partial q^*/\partial t$ are obtained from (20). Equation (6) is satisfied if

$$\gamma(e) = 0, \tag{24}$$

for $e = \pm\infty$. The initial/boundary-value problem defined by (1)–(9) is solved if the functions z_F and γ along the free surface and the function σ along the cylinder contour are obtained as functions of time. These functions satisfy a system of three differential evolution equations, parameterized by e and θ, consisting of (21) for the free surface and equations for the vortex strength and source strength in the form of Fredholm integral equations of the second kind, equations (22) and (23). The corresponding initial conditions are

$$z_F(e, t = 0) = e, \tag{25}$$

$$\gamma(e, t = 0) = 0, \tag{26}$$

$$\sigma(\theta, t = 0) = 0. \tag{27}$$

Since the free surface is infinitely long, it is necessary to introduce wave damping to reduce to a finite length the part for which computation is required. The free-surface vortex density and height are set to zero outside the region $|x| < x_R$, and in the region $|x| < x_R$ the free-surface position and the vortex density along the free surface obey the modified evolution equations

$$\frac{\partial x_F}{\partial t}(e) = R_1; \tag{28}$$

$$\frac{\partial y_F}{\partial t}(e) = I_1 - D_F\,|x_F(e)| - x_D|\,y_F(e); \tag{29}$$

$$\frac{\partial \gamma}{\partial t}(e) = R_2 - D_F\,|x_F(e)| - x_D|\,\gamma(e). \tag{30}$$

$R_1 - iI_1$ is the right-hand side of (21), and R_2 is the right-hand side of (22). Here D_F is zero if $|x| < x_D$ and D_F is non-zero if $x_D < |x| < x_R$. Thus there is a region $|x| < x_D$ in which (28)–(30) reduce to the undamped equations (21) and (22), a region $x_D < |x| < x_R$ where waves entering from $|x| < x_D$ are damped, and a region $|x| > x_R$ where the water remains undisturbed. Computations can then be restricted to $|x| < x_R$. In all cases of computations with a free surface present, $x_R = 10.0$, $x_D = 7.5$, and $D_F = 0.8$. This damping is different from that used by Baker *et al.* (1981) only in that the damping factor $D_F\,|x_F(e)| - x_D|$ varies linearly instead of quadratically, as is the case with their damping factor $\nu(x)$. The damping terms in (29) and (30) are continuous in the truncated region $|x| < x_R$. For this free-surface flow problem, the time for which the flow is simulated is the finite time it takes the cylinder to rise to the free surface. Thus one does not expect significant waves to reach the damping regions.

For the case of a rigid wall replacing the free surface, the complex velocity potential is expressed solely in terms of a layer of sources on the cylinder and another layer of sources on the reflection of the cylinder about the wall:

$$w(z) = \frac{1}{2\pi}\int_0^{2\pi} \sigma(\theta')\log(z - z_B(\theta'))\,d\theta' + \frac{1}{2\pi}\int_0^{2\pi} \sigma(\theta')\log(z - z_B^*(\theta'))\,d\theta'. \tag{31}$$

The wall boundary condition, equation (14), is then automatically satisfied. The evolution equation for the source strength along the cylinder contour is derived from (5) and assumes the form

$$\frac{\partial \sigma}{\partial t}(\theta) = 2\ddot{y}_c \sin(\theta) + Re\left\{\frac{iz_B'(\theta)}{\pi}\left[\int_0^{2p} \frac{\partial\sigma/\partial t(\theta')}{z_B(\theta) - z_B(\theta')}\,d\theta' + \int_0^{2\pi} \frac{\partial\sigma/\partial t(\theta')}{z_B(\theta) - z_B^*(\theta')}\,d\theta' - 2i\dot{y}_c\int_0^{2\pi} \frac{\sigma(\theta')}{[z_B(\theta) - z_B^*(\theta')]^2}\,d\theta'\right]\right\}. \tag{32}$$

The initial/boundary-value problem for the case of a rigid wall is solved once the source strength σ along the cylinder contour has been determined as a function of time. This function is sought as the solution of the parameterized differential equation (32) which is a Fredholm integral equation of the second kind for the time derivative of the source strength. The initial condition is specified by (27).

The functions $z_F(e, t)$ and $\gamma(e, t)$ are discretized spatially by defining the functions

$$(z_F)_j(t) \equiv (x_F)_j(t) + i(y_F)_j(t) = z_F(e_j, t), \tag{33}$$

and

$$\gamma_j(t) = \gamma(e_j, t), \tag{34}$$

where $t \geqslant 0$ and $j = 1, 2, \ldots, N$. The initial definition of these discretized functions is given by

$$(z_F)_j(0) \equiv (x_F)_j(0) + i(y_F)_j(0) = [j - \tfrac{1}{2}(N+1)]\,\Delta e, \tag{35}$$

and

$$\gamma_j(0) = 0. \tag{36}$$

The increment Δe and N, an odd integer, are chosen so that $e_1 = -x_R$ and $e_N = x_R$. The functions $z_B(\theta, t)$ and $\sigma(\theta, t)$ are discretized analogously by defining

$$(z_B)_k(t) \equiv (x_B)_k(t) + i(y_B)_k(t) = z_B(\theta_k, t), \tag{37}$$

and

$$\sigma_k(t) = \sigma(\theta_k, t), \tag{38}$$

for $k = 1, 2, \ldots, M$. Here θ_k are given by

$$\theta_k = (k - \tfrac{1}{2})\,(2\pi/M), \tag{39}$$

and $(z_B)_k(t)$ are equal to

$$(z_B)_k(t) = z_B(\theta_k, t). \tag{40}$$

For each j, the functions $(z_F)_j(t)$ and $\gamma_j(t)$ obey ordinary differential equations obtained from (28)–(30) by discretizing the right-hand sides spatially. The integrals are replaced by sums based on trapezoidal quadrature, and spatial derivatives with respect to e are computed using a cubic-spline technique. Typical of this discretization is the replacement of the principal-value integral

$$\int_{-\infty}^{\infty} \frac{\gamma(e')\,de'}{z_F(e) - z_F(e')}$$

found in (20) by the sum

$$2\sum \frac{\gamma_k\,\Delta e}{(z_F)_j - (z_F)_k},$$

in which e and e' are associated with the indices j and k respectively. The summation is over the even values of k if j is odd and over the odd values of k if j is even. Similarly, regular integrals such as

$$\int_0^{2\pi} \frac{\sigma(\theta')}{z_F(e) - z_B(\theta')}\,d\theta'$$

in (20) are replaced by sums of the form

$$\sum_{j=1}^{M} \frac{\sigma_k\,\Delta\theta}{(z_F)_j - (z_B)_k}.$$

For each k, the function $\sigma_k(t)$ obeys an ordinary differential equation obtained from (23) or, for the case of the rigid wall, equation (32). The ordinary differential equations for $\gamma_j(t)$ and $\sigma_k(t)$ are Fredholm integral equations of the second kind with eigenvalues that guarantee the convergence of an iterative solution technique for

their derivatives (Baker *et al.* 1982). The rate of convergence depends on the depth of the cylinder with the convergence becoming slower as the cylinder moves toward the free surface. Convergence, however, can be maintained by reducing the timestep and thus ensuring that the initial estimates of the solutions of the integral equations are better and require fewer iterations to achieve convergence. The functions $(z_B)_k(t)$ are calculated from $y_c(t)$, which is defined by (10)–(12). The result of the discretization process is a coupled nonlinear system of ordinary differential equations for the functions $(z_F)_j(t)$, $\gamma_j(t)$, and $\sigma_k(t)$. When the free surface is replaced by a rigid wall, only $\sigma_k(t)$ appears in the system of equations. There are $3N+M$ equations in this system when a free surface is present and M equations for the rigid-wall case.

The initial depth d of the circular cylinder, found in (10), was set equal to 5. This is deep enough so that the free surface is essentially undisturbed by starting transients. The number of free-surface points N was set to 321; the free-surface increment Δe is 0.0625. The cylinder contour was discretized in such a way that the number of sources on the cylinder, M, was 100. In this arrangement the initial spacing between sources on the cylinder and vortices on the free surface was about the same.

Two methods have been used to solve the system of differential equations. One is an implicit fourth-order Adams–Bashforth–Moulton predictor–corrector scheme with a fixed timestep. The first few timesteps are treated with an explicit fourth-order Runge–Kutta technique. The other method of solving the system of equations numerically is to use the subroutine DEABM (Shampine & Watts 1979). DEABM is a variable-order, variable-step integrator that determines the solution for each step in such a way that specified local error criteria are met. Thus one can use DEABM to determine a solution using timesteps of an appropriate size so that the solution meets specified error criteria without knowing in advance what that step size should be. The information gained about the appropriate step size can be used to recompute the solution using the fixed-step, fixed-order method. When a rigid wall replaced the free surface, only the subroutine DEABM was used.

With either method of time integration, numerical instabilities arise on the computed free surface if a filtering scheme is not used. In particular, it has been found that, if linear filtering is not used in conjunction with DEABM, rather large step sizes are chosen and the computed free surface is not smooth. The numerical filtering scheme, which involves filtering the (x, y)-parameterization of the free surface and the vortex strength along the free surface, is employed immediately after the predictor in DEABM in each timestep. Filtering was discussed by Shapiro (1975) and has been used by Longuet-Higgins & Cokelet (1976) and Haussling & Coleman (1979) to eliminate numerical instabilities on a free surface. When a solution was recomputed using the fourth-order fixed-step method with a timestep of about the same size as used by DEABM and with smoothing between each timestep, very little difference was noticed. Thus, the procedure involving DEABM produces solutions in agreement with the solutions from the fixed-order, fixed-step method if an appropriate step size is chosen.

A numerical check of the accuracy of the computations is obtained from comparing the calculated rate at which the total energy in the fluid is changing with the calculated rate at which work is performed on the fluid by the body. The total energy in the fluid is normalized by $\rho U^2 R^2$ and is the sum of the potential energy of the fluid, given by

$$\mathrm{PE} = \frac{1}{2Fr^2}\int_{-\infty}^{\infty} y_F^2(e')\, x_e(e')\, \mathrm{d}e' - \frac{\pi y_c(t)}{Fr^2}, \tag{41}$$

and the kinetic energy in the fluid, given by

$$\mathrm{KE} = \frac{1}{2}\int_{-\infty}^{\infty} \phi(\phi_x n_x + \phi_y n_y)\, s_e(e')\, \mathrm{d}e' - \frac{1}{2}\int_0^{2\pi} \phi(\phi_x n_x + \phi_y n_y)\, \mathrm{d}\theta'. \tag{42}$$

In each of these two equations, the first term is a free-surface integral in which $n_x + \mathrm{i}n_y$ is the unit normal vector directed away from the fluid region. These terms vanish in the rigid-wall case. The fluid velocity $\phi_x - \mathrm{i}\phi_y$ on the free surface in the first integral of (42) is the velocity $\tilde{q}^*$ of (21). The second term in (42) is a body integral with the unit normal vector directed into the fluid region. The fluid velocity on the body in this integral is obtained by differentiating (19), or (31) for the rigid-wall case, with respect to z and taking the limit as z approaches the body from inside the fluid. The potential ϕ on the free surface and on the cylinder may also be obtained from (19) or (31). The rate at which energy is supplied to the fluid is equal to the rate of work done by the body on the fluid. It is normalized by $\rho U^3 R$ and given by the equation

$$\frac{\mathrm{d}E}{\mathrm{d}t} = \frac{-\pi \dot{y}_c(t)}{Fr^2} + \dot{y}_c(t)\int_0^{2\pi} p_d(\theta') \sin\theta'\, \mathrm{d}\theta'. \tag{43}$$

The dynamic pressure p_d in this equation is obtained, after accounting for the fact that the body is moving, by the formula

$$p_d(\theta) = -\frac{\partial\phi}{\partial t} + \phi_x(\dot{x}_B - \tfrac{1}{2}\phi_x) + \phi_y(\dot{y}_B - \tfrac{1}{2}\phi_y). \tag{44}$$

Here the first derivative on the right-hand side of the equation is the derivative of ϕ with respect to t for fixed θ. It is calculated from a formula based on (19) or (31). All of these relations involve integrals that are evaluated from formulae based on trapezoidal quadrature. The total energy is computed at fixed intervals of time and then numerically differentiated with respect to time. The result of the numerical differentiation is compared with the calculated rate at which work is performed on the fluid.

4. Results

The method just described has been used to solve the free-surface flow problem for four cases in which $1/Fr^2 = 0.5$, 5.0, 25.0, and 100.0 and the rigid-wall problem. Equations (22), (23), and (32) for $\partial\gamma/\partial t$ and $\partial\sigma/\partial t$ are Fredholm integral equations of the second kind. The discretized forms of these equations are solved iteratively using their convergent Neumann series (Baker *et al.* 1981). For the free-surface cases, separate global error criteria were used to test for the convergence of $\partial\gamma_j/\partial t$ and $\partial\sigma_k/\partial t$. The criteria were obtained experimentally and were such that the difference in two successive iterates was nearly equal to the limit in numerical accuracy that could be attained with this spacing of points on the free surface and cylinder. In particular, the root mean square of the change in two successive iterates had to be less than prescribed tolerances. The prescribed tolerances were initially equal to 5×10^{-5} except in the case of $1/Fr^2 = 100$ when the more stringent tolerance 5×10^{-6} was used initially. The tolerances were increased by 10 % each time the number of iterations exceeded 15, which usually indicated that $\partial\gamma_j/\partial t$ or $\partial\sigma_k/\partial t$ had become relatively large. In most cases, the tolerances were not increased until the cylinder came very close to the free surface. For the rigid-wall case, a local error criterion was used at each point; the absolute value of the difference in two successive iterates had

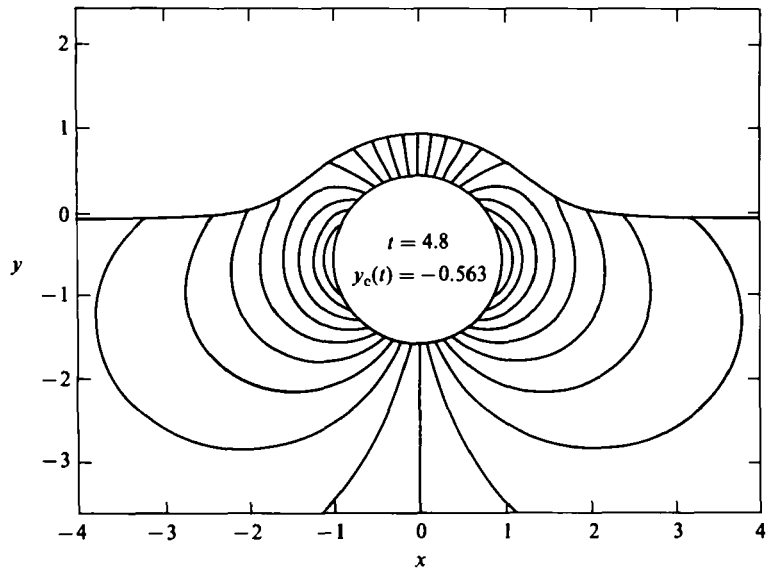

FIGURE 2. Streamlines $\psi = -0.9, -0.8, \ldots, 0.9$ at $t = 4.8$ for $1/Fr^2 = 0.5$.

to be less than 10^{-5} plus 10^{-4} times the absolute value of the latest iterate at each point.

For the case $1/Fr^2 = 0.5$ both the variable-step, variable-order integrator DEABM and the fixed-step, fixed-order method were used. For DEABM, the time-discretization error specified for x- and y-positions on the free surface and on the cylinder was a combination of an absolute and a relative error. In particular, the error estimated by DEABM at each point had to be less than 10^{-5} plus 10^{-4} times the absolute value of the computed solution at the point. The same error criterion was used for the time-advancement of the source strength σ on the cylinder and the vortex strength γ on the free surface. In this particular case of $1/Fr^2 = 0.5$, the global error tolerance for $\partial\gamma_j/\partial t$ was maintained at 5×10^{-5}, whereas the global error tolerance for $\partial\sigma_k/\partial t$ was increased gradually from 5×10^{-5} to 6.7×10^{-5} for $t > 5$ after being fixed up to that time. Even with such necessary relaxation of the convergence criterion for $\partial\sigma_k/\partial t$, the rate of change of energy with respect to time and the rate at which work was performed on the fluid remained in good agreement. The timestep chosen by DEABM was 0.16 for t between 1.5 and 3.5. For larger times, the step size was gradually decreased to 0.04 at $t = 5.5$. The order of the method was four at early times, eight near $t = 4$, and five near the end of the calculation. With this information, the calculation was repeated using the fixed-step, fourth-order Adams–Bashforth–Moulton scheme and a timestep of 0.01. It was found that the calculated energy in the fluid and the calculated rate of work performed on the fluid by the cylinder were unchanged in the four most significant digits. Thus, the methods produced results in agreement with one another.

Figures 2–4 show the free surface, the cylinder, and streamlines in the fluid about the cylinder for three times as the cylinder approaches the free surface. These correspond to the times 4.8, 5.3, and 5.8. The plotted streamlines are contour lines for ψ equal to 0.0, 0.1, ..., 0.9 in the right-hand half of each figure and the negative of these values in the left-hand half of each figure. The computation could not be continued accurately much beyond $t = 5.8$ because after this time the distance

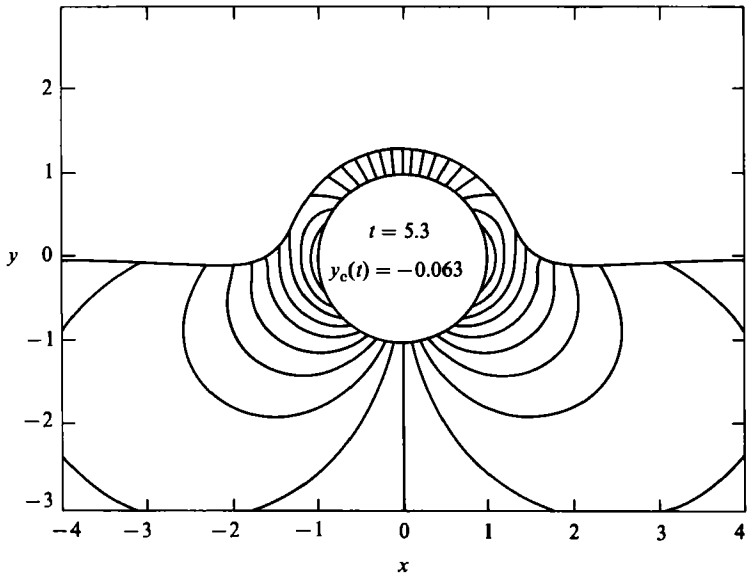

FIGURE 3. Streamlines $\psi = -0.9, -0.8, \ldots, 0.9$ at $t = 5.3$ for $1/Fr^2 = 0.5$.

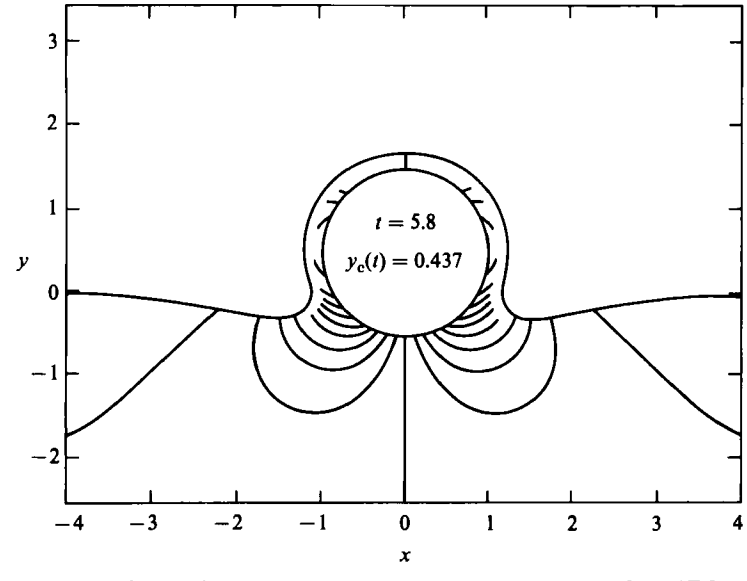

FIGURE 4. Streamlines $\psi = -0.9, -0.8, \ldots, 0.9$ at $t = 5.8$ for $1/Fr^2 = 0.5$.

between the free surface and the cylinder contour becomes less than the spacing between the vortices on the free surface and the spacing between the sources on the cylinder contour. When this happens, local effects of the individual sources and vortices predominate in the region between the cylinder and the free surface. This is the case of motion in which the final velocity of the rising cylinder is largest and the ratio of the inertial forces to the gravitational force is quite large. The large inertial forces are reflected in the appearance of the streamlines which resemble, especially at the earlier times, those of a cylinder moving at constant speed in an

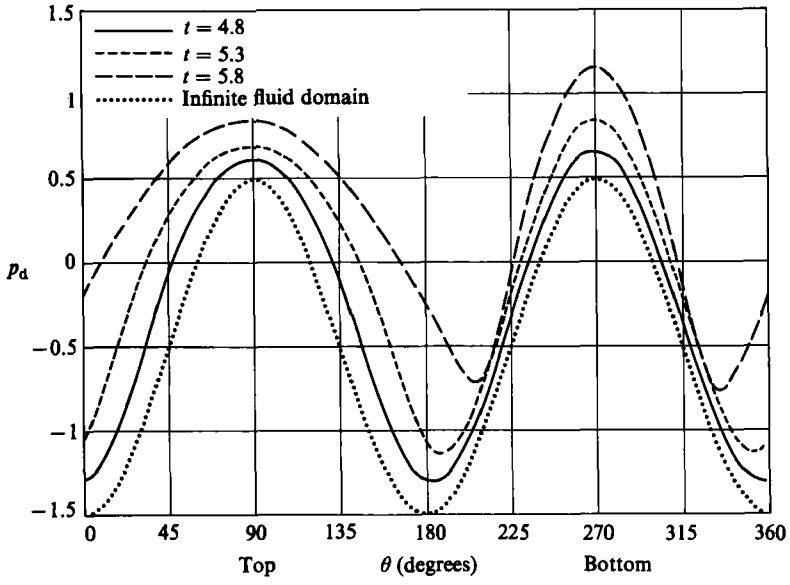

FIGURE 5. Dynamic pressure on the cylinder at $t = 4.8$, 5.3, and 5.8 for $1/Fr^2 = 0.5$ and for an infinite fluid domain.

infinite fluid. The free surface is pushed away rapidly by the flow, does not have time to respond much to the restoring influence of gravity, and hence exerts a minor influence on the streamlines.

Figure 5 presents the dynamic pressure on the cylinder for these three times and the pressure on a steadily moving cylinder in an infinite fluid. For the earliest time, the pressure distribution resembles the pressure distribution for the case of a cylinder moving in steady motion in an infinite fluid. At this time the pressure exhibits an up/down symmetry in addition to the right/left symmetry which is inherent. At later times the up/down symmetry is lost. The pressure is increasing with time at every point on the cylinder and forms a relatively sharp peak at $\theta = 270°$, the lowest point on the cylinder. The minima on either side of this peak have moved closer to $\theta = 270°$. This seems to reflect the fact that an increasingly greater portion of the cylinder is surrounded by a thin layer of fluid between the free surface and the cylinder, as can be seen in figure 4.

Figures 6–8 present the cylinder, the free surface, and the streamlines at the times 4.0, 4.24, and 4.52 as the cylinder moves to the free surface with a speed such that $1/Fr^2 = 5.0$. The same values of the stream function are plotted as for the previous case. The computation has again been carried out to the point at which the distance between the free surface and the cylinder is about equal to the spacing between successive vortices on the free surface and successive sources on the cylinder contour. In this case the fourth-order fixed-step method was used after an experimental computation had been performed with DEABM. For $0 \leqslant t \leqslant 3.8$, the timestep was 0.02, and for larger times it was 0.01. A noticeable difference between the results for this speed and for the previous speed is that in this case the streamlines are deflected downward by the free surface from those streamlines corresponding to a circular cylinder moving steadily in an unbounded fluid. Also, the free surface is not disturbed as much by the rising cylinder for $1/Fr^2 = 5.0$. This is a reflection of the relatively stronger acceleration of gravity compared with inertial forces in this case. Since the

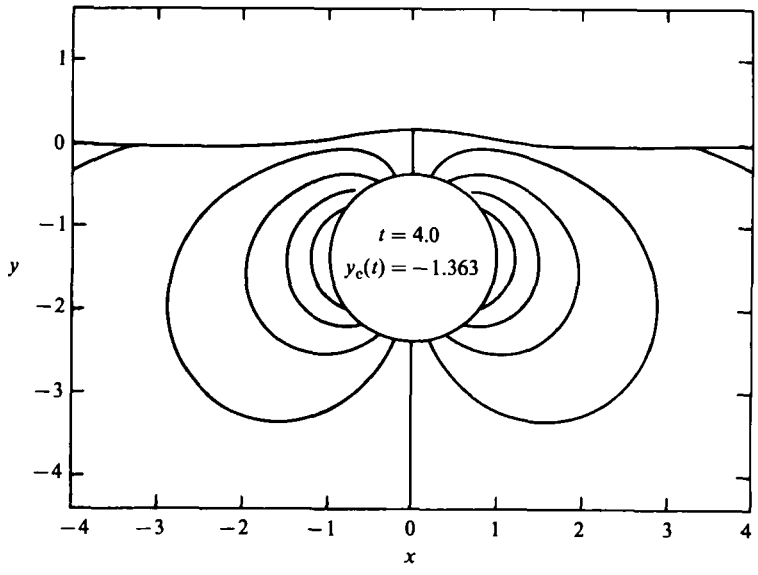

FIGURE 6. Streamlines $\psi = -0.9, -0.8, \ldots, 0.9$ at $t = 4.0$ for $1/Fr^2 = 5.0$.

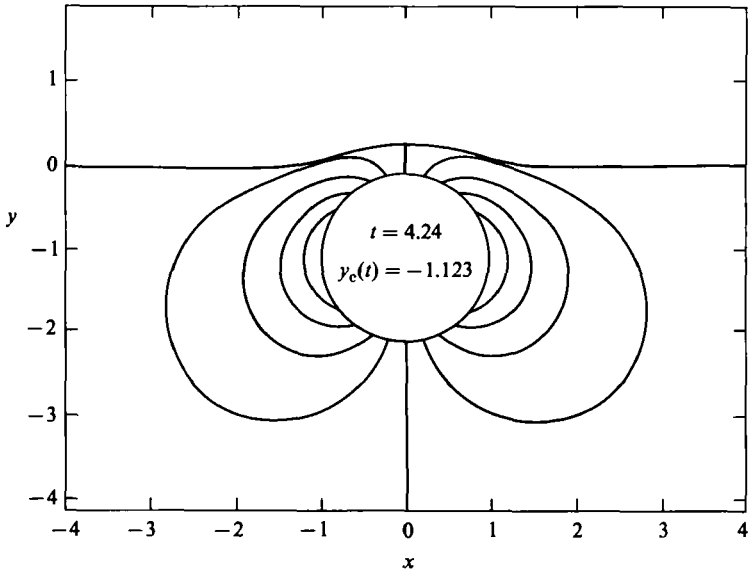

FIGURE 7. Streamlines $\psi = -0.9, -0.8, \ldots, 0.9$ at $t = 4.24$ for $1/Fr^2 = 5.0$.

body is rising more slowly, the restoring force of gravity has time to act and prevent the free surface from becoming highly distorted. Gravity wave motion is apparent in the figures. A plot of the dynamic pressure distribution on the cylinder is depicted in figure 9 for $t = 4.0$, 4.24, and 4.52 and for the case of a steadily moving cylinder in an infinite fluid. In this figure, as the cylinder nears the free surface, the pressure at the closest point to the free surface ($\theta = 90°$) is increasing and deviating considerably from that for the cylinder in an infinite fluid. At the point farthest from the free surface the pressure changes only very little from the infinite-fluid pressure.

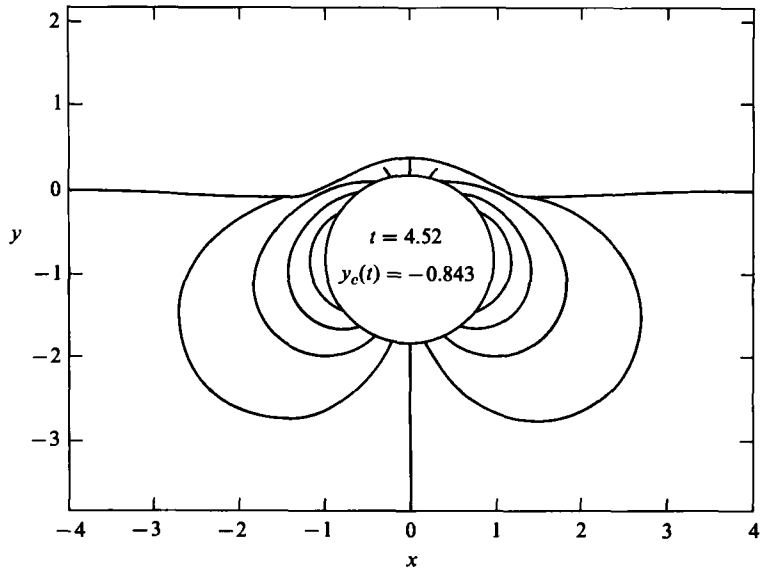

FIGURE 8. Streamlines $\psi = -0.9, -0.8, \ldots, 0.9$ at $t = 4.52$ for $1/Fr^2 = 5.0$.

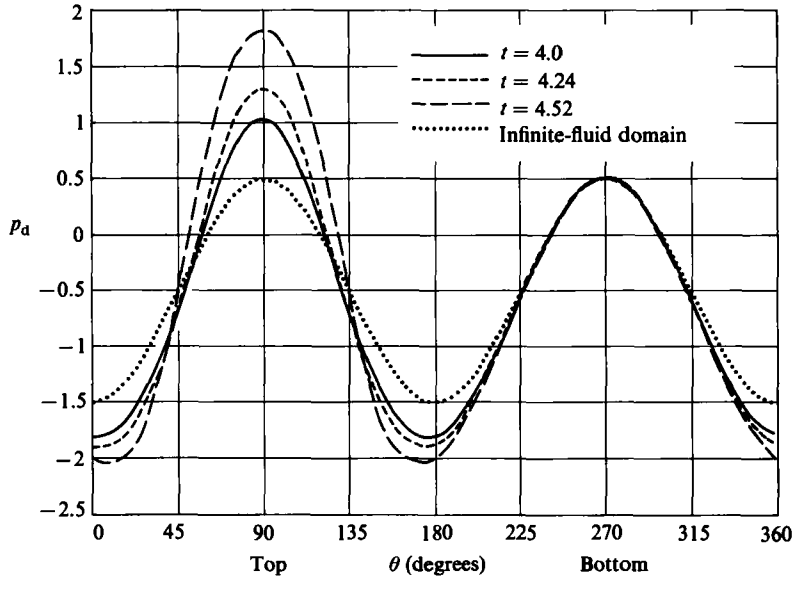

FIGURE 9. Dynamic pressure on the cylinder at $t = 4.0$, 4.24, and 4.52 for $1/Fr^2 = 5.0$ and for an infinite fluid domain.

The final case for which results are presented in the form of contour plots of the stream function is for $1/Fr^2 = 25$. In this case the fourth-order, fixed-step method was used again. For $0 \leqslant t \leqslant 4.0$ the timestep used was 0.02; for larger times it was 0.01. The global convergence criteria for both $\partial\gamma_j/\partial t$ and $\partial\sigma_k/\partial t$ were 5×10^{-5} at all times for this case. Of the three cases presented so far, this is the case of slowest motion of the cylinder. Figures 10–12 present the free surface, the cylinder, and the streamlines for $t = 3.76$, 4.04, and 4.24. As before, the streamlines are plotted for ψ

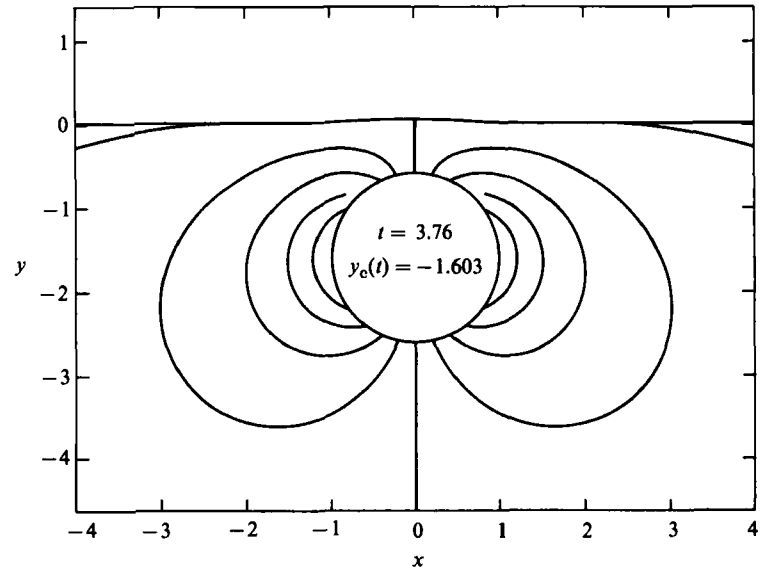

FIGURE 10. Streamlines $\psi = -0.9, -0.8, \ldots, 0.9$ at $t = 3.76$ for $1/Fr^2 = 25.0$.

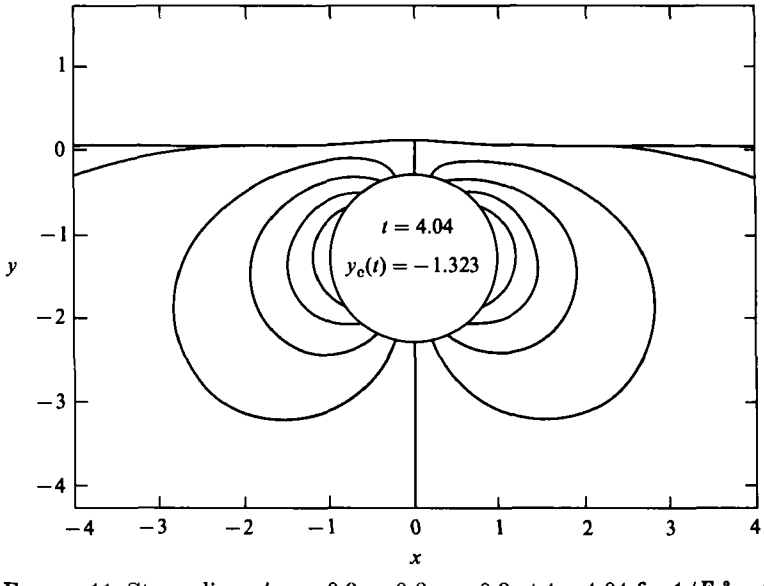

FIGURE 11. Streamlines $\psi = -0.9, -0.8, \ldots, 0.9$ at $t = 4.04$ for $1/Fr^2 = 25.0$.

equal to $-0.9, -0.8, \ldots, 0.9$. The results indicate that the free surface is scarcely deflected by the rising cylinder and that the streamlines deviate considerably from the streamlines for steady-state movement of a circular cylinder in an infinite fluid. The flow in this case is very close to that for the cylinder approaching a rigid wall. Figure 13 shows the variation of the dynamic pressure on the cylinder as a function of θ for $t = 3.76$, 4.04, and 4.24. For this case the pressure near $\theta = 90°$, the topmost point on the cylinder, is increasing rapidly to form a pronounced peak, whereas over much of the cylinder the pressure oscillates near the infinite-fluid pressure. Evidence

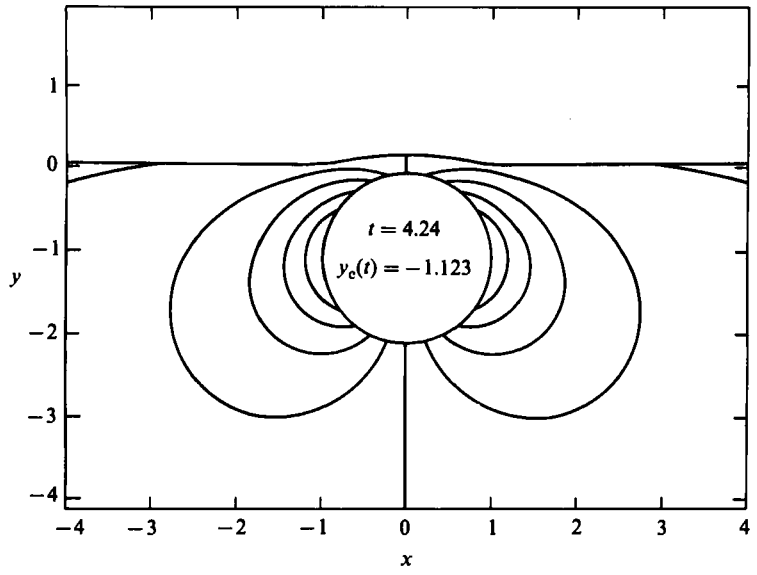

FIGURE 12. Streamlines $\psi = -0.9, -0.8, \ldots, 0.9$ at $t = 4.24$ for $1/Fr^2 = 25.0$.

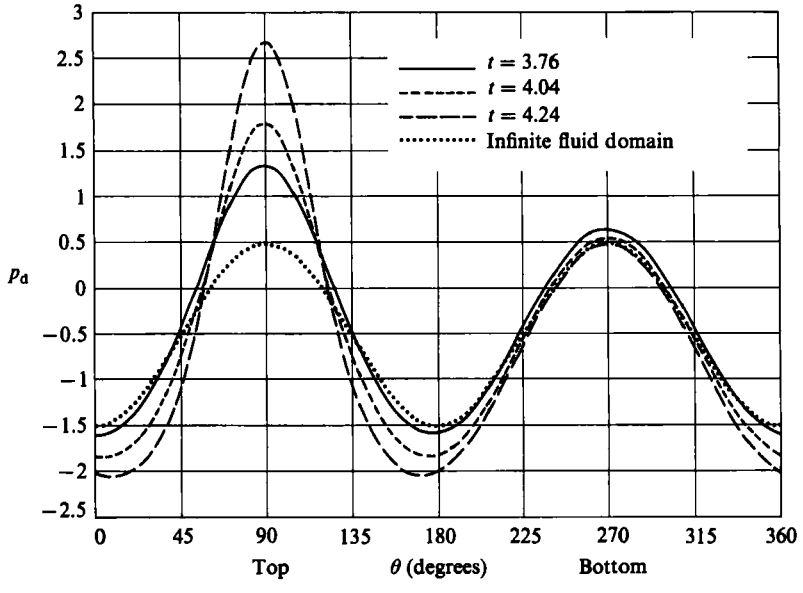

FIGURE 13. Dynamic pressure on the cylinder at $t = 3.76$, 4.04, and 4.24 for $1/Fr^2 = 25.0$ and for an infinite fluid domain.

of this oscillation can be seen at the bottom of the cylinder, where at $t = 4.24$, the pressure is approaching the pressure for the infinite-fluid case which it was near at earlier time. At the sides of the cylinder the pressure is moving away from that which is expected for a steadily moving cylinder in an infinite fluid.

Similar calculations have been performed for the circular cylinder approaching a rigid wall. The computed pressure distribution on the cylinder at $t = 2.5$, 3.0, 3.5, and 4.0 is depicted in figure 14 together with the pressure distribution on a steadily

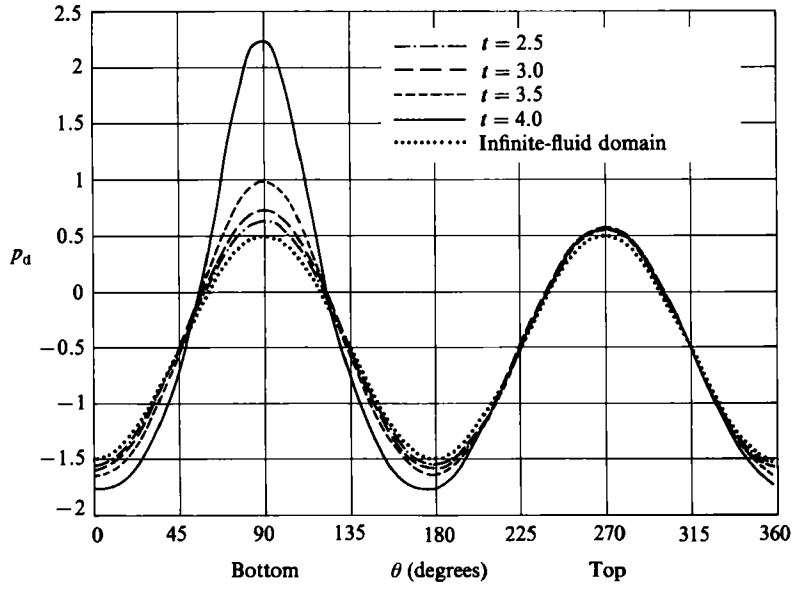

FIGURE 14. Dynamic pressure on the cylinder at $t = 2.5$, 3.0, 3.5, and 4.0 for a rigid wall in place of the free surface and for the case of an infinite fluid domain.

moving cylinder in an infinite fluid. At the earliest time the pressure is not far from the pressure on the cylinder in an infinite fluid. As the cylinder moves closer to the free surface, the pressure at the topmost point on the cylinder rises to a sharp peak, decreases slightly at the sides of the cylinder, and remains essentially unchanged at the bottom of the cylinder. The behaviour of the pressure distribution is similar to the behaviour of the pressure distribution depicted in figure 13 for the free-surface flow in which $1/Fr^2 = 25.0$. For that free-surface flow problem, the pressure peak on top of the cylinder is not as pronounced and the pressure on the bottom of the cylinder is more variable.

Another calculation has been performed for a free-surface flow in which the final speed of approach to the free surface is such that $1/Fr^2 = 100$. The streamlines are not presented for this case since they are very similar to those for $1/Fr^2 = 25$. The dynamic force as a function of time for all four free-surface flow problems and the rigid-wall problem is depicted in figure 15. For $0 < t < 1$, the period during which the cylinder is undergoing acceleration from rest, the computed force is essentially equal to the acceleration reaction experienced by a cylinder accelerating in an infinite fluid (Batchelor 1967). In the high-speed case ($1/Fr^2 = 0.5$) the force is essentially zero after the acceleration period as for a body in an infinite fluid. As the body nears the free surface a downward force then develops and is increasing in strength at the termination of the calculations. Thus this inviscid flow theory predicts a monotonically increasing resistance when a cylinder is raised rapidly to a free surface at a constant speed. The force curves for the slower speed cases exhibit similar behaviour except that they show oscillations in time due to the surface wave motion. For $1/Fr^2 = 25$ and 100, there are time intervals during which the force is upward, a negative resistance. With decreasing Froude number the oscillations increase in frequency and the force curves approach and oscillate about the rigid-wall force.

The free-surface wave motion is depicted in figure 16. This figure shows the height

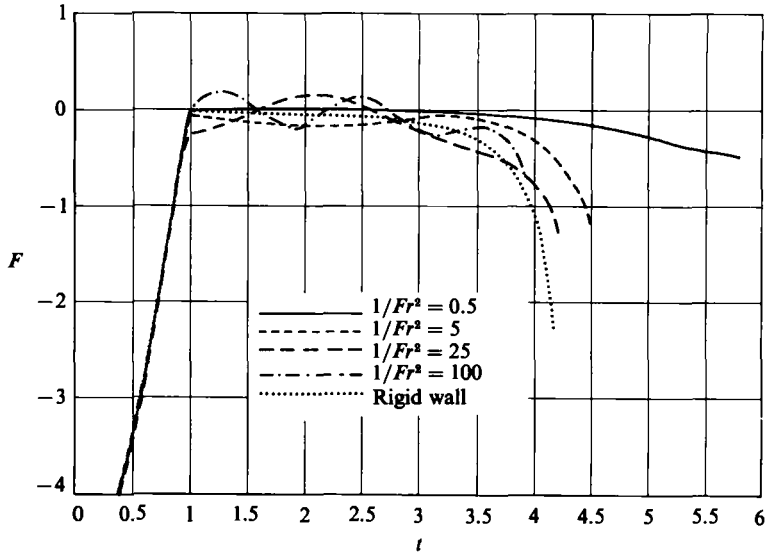

FIGURE 15. Dynamic force on the cylinder versus time.

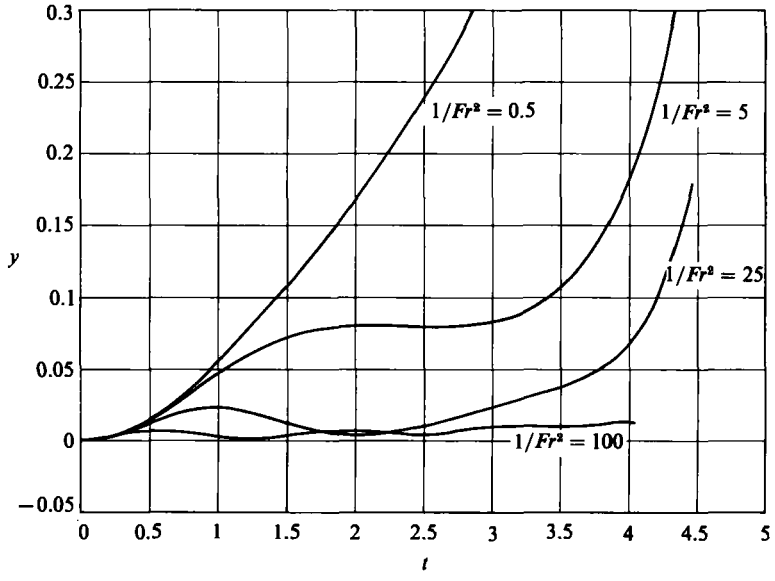

FIGURE 16. Free-surface elevation directly above the cylinder versus time.

of the free surface directly above the cylinder as a function of time for the four speeds of approach. Whereas the high-speed approach shows no wave motion, the other curves do show some vertical oscillation of the free surface. The period of these oscillations decreases as the Froude number decreases. The amplitude increases at first and then decreases. When the cylinder is very close to the free surface, the free surface abruptly rises. In the slow-speed approach, the calculations had to be terminated before the rise because it occurs only after the cylinder comes extremely close to the surface.

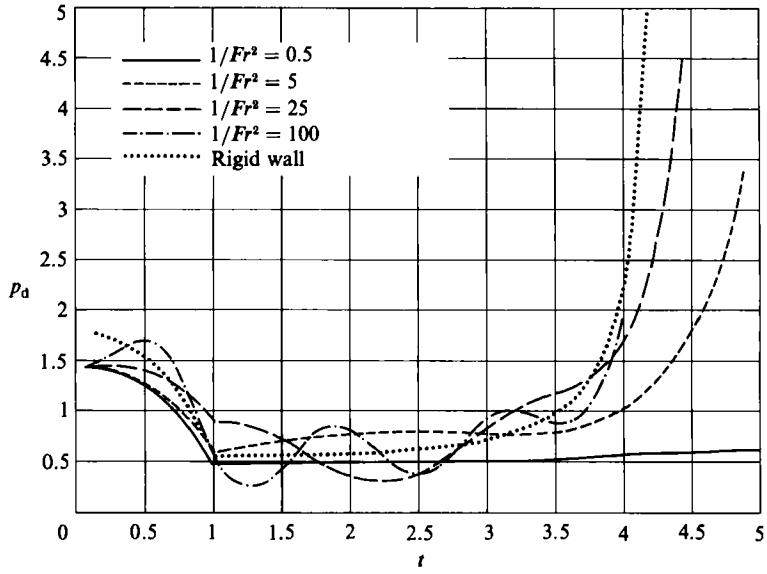

FIGURE 17. Dynamic pressure on the top of the circular cylinder ($\theta = 90°$) versus time.

Figures 17 and 18 show the pressure at the top and the bottom of the cylinder as functions of time for the four cases of free-surface flow and for the case of flow when the free surface is replaced by a rigid wall. From figure 17 one can see that in the high-speed approach the pressure remains very close to the pressure for the cylinder in an infinite fluid ($p_d = 0.5$). At the slow-speed extreme, obtained by replacing the free surface by a rigid wall, the pressure begins to rise gradually and then rises abruptly as the cylinder approaches the wall. For intermediate Froude numbers, the pressure oscillates before it experiences the final abrupt rise. In figure 18, one can see that the pressure at the bottom of the cylinder in the high-speed approach is not much different from the pressure in the rigid-wall case. Both are near the pressure at that point on a cylinder in an infinite fluid ($p_d = 0.5$), and both show a gradual rise as a function of time. The pressure at the bottom of the cylinder at intermediate Froude numbers shows the same oscillatory behaviour as at the top of the cylinder. At both the top and the bottom of the cylinder, the pressure oscillations approach the pressure for the rigid-wall case and the frequency of oscillation increases with decreasing Froude number.

For these flows, the degree of agreement of the calculated rate of change of the total energy in the fluid with the calculated rate at which work is performed on the fluid by the cylinder was used as an indicator of the numerical accuracy. For the rigid-wall case, these two quantities were within 2 % of one another when $0 < t < 3$. The discrepancy increased to 3.5 % at $t = 4$ near the end of the calculation. In all the free-surface cases, the numerical error was so small that the computed rate of change of energy in the fluid was close to the calculated rate at which work was performed by the body on the fluid. For the case in which $1/Fr^2 = 0.5$, the difference in these two quantities remained small enough so that even near the end of the calculation, at $t = 5$, they were only about 2 % apart. For slower speeds of approach to the free surface, the difference in the two quantities was greater, and the two quantities oscillated about one another. Even for $1/Fr^2 = 100.0$, the case in which the discrepancy was greatest, the difference between the two quantities averaged only

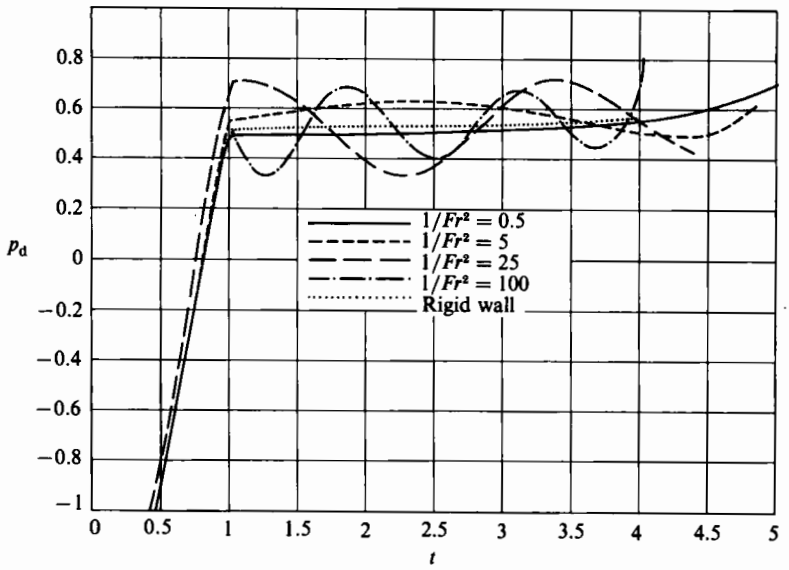

FIGURE 18. Dynamic pressure on the bottom of the circular cylinder ($\theta = 270°$) versus time.

5% although at one time it was as high as 15%. The timestep was halved, but the computed rate of change of the total energy in the fluid and the computed rate of change of the work performed on the fluid by the cylinder did not change significantly. Thus this error is not due to the time integration, but is due to inadequate spatial resolution of small-amplitude, short-wavelength waves which can contain significant energy at low speeds.

5. Summary

The problems of the flow about a circular cylinder rising to a free surface and a rigid wall have been solved numerically. Streamlines and pressures have been used to compare the approach to a free surface with the approach to a rigid wall and to motion in an infinite fluid. It has been shown that the low-speed approach to the free surface is essentially the same as the approach to a wall while the high-speed approach is similar to motion in an infinite fluid. At intermediate speeds surface wave motion is evident. In all cases, the cylinder experiences a growing downward force as it nears the free surface or wall except that short periods of upward force occur when wave motion is significant.

This work was supported by the Numerical Naval Hydrodynamics Program at the David W. Taylor Naval Ship Research and Development Center. This programme is sponsored jointly by the Independent Research Program at DTNSRDC and the Office of Naval Research.

REFERENCES

BAKER, G. R., MEIRON, D. I. & ORSZAG, S. A. 1981 Applications of a generalized vortex method to nonlinear free surface flows. *Proc. Third Intl Conf. on Numerical Ship Hydrodynamics*. Paris.

BAKER, G. R., MEIRON, D. I. & ORSZAG, S. A. 1982 Generalized vortex methods for free-surface flow problems. *J. Fluid Mech.* **123**, 477–501.

BATCHELOR, G. K. 1967 *An Introduction to Fluid Dynamics*. Cambridge University Press.

GREENHOW, M. & LIN, W-M. 1983 Nonlinear free surface effects: experiments and theory. *MIT Rep.* 83–19.

GREENHOW, M. & LIN, W-M. 1985 Numerical simulation of nonlinear free surface flows generated by wedge entry and wavemaker motions. *Proc. Fourth Intl Conf. on Numerical Ship Hydrodynamics*. Washington, DC.

HAUSSLING, H. J. & COLEMAN, R. M. 1979 Nonlinear water waves generated by an accelerated circular cylinder. *J. Fluid Mech.* **92**, 767–781.

LIN, W-M., NEWMAN, J. N. & YUE, D. K. 1984 Nonlinear forced motions of floating bodies. *Proc. 15th Symp. on Naval Hydrodynamics*. Hamburg, Germany.

LONGUET-HIGGINS, M. S. & COKELET, E. D. 1976 The deformation of steep surface waves. I. A numerical method of computation. *Proc. R. Soc. Lond.* A **350**, 1–26.

SHAMPINE, L. F. & WATTS, H. A. 1979 DEPAC-Design of a user oriented package of ODE solvers. *Sandia Laboratories Rep.* SAND79-2374.

SHAPIRO, R. 1975 Linear filtering. *Math. Comp.* **29**, 1094–1097.

VINJE, T. & BREVIG, P. 1981 Nonlinear, two-dimensional ship motion. *Ship Res. Inst. of Norway, Rep.* 112.81.